TO: NATIONAL AERONAUTICS AND SPACE ADMINISTRATION
LEWIS RESEARCH LABORATORIES
BROOKPARK
CLEVELAND, OHIO
ATTN: DR. R. D. PRIEM

FROM: DR. B. A. REESE
JET PROPULSION CENTER
PURDUE UNIVERSITY
LAFAYETTE, INDIANA

NGR-15-005-058

SUBJECT: SEMI-ANNUAL PROGRESS REPORT FOR THE PERIOD JULY 1 TO DECEMBER 1 1968 ~~1969~~. THE WORK ACCOMPLISHED DURING THIS PERIOD WILL BE REPORTED UNDER THE FOLLOWING HEADINGS:

Task 1. Performance Investigation

Task 2. Heat Transfer Investigation

Task 3. Combustion Stability Investigation

I. Introduction

During this report period effort has been concentrated in the following areas.

A. An analysis of the data obtained from the initial twenty-four experimental firings has been conducted to determine the effects of nozzle throat erosion and flow separation on the performance of the experimental rocket motor.

B. The correlation of heat with mass transfer was investigated for the indirect determination of nozzle heat flux from ablation rates.

C. Several experimental firings of the 4000 psi experimental combustion chamber were conducted to test the pulse gun and pulse gun circuitry. A summary of the alterations required for pulsing the engine is included.

II. Status of the Work in Progress

A. Task 1. Performance Investigation

Performance data has been recorded from twenty four experimental firings of a rocket engine operated at 4000 psi. This data will be compared with tabulated theoretically predicted performance to determine the effects of chamber pressure, mixture, ratio, injector configuration and characteristic length on combustion efficiency and thrust. Initial analysis of the data indicated that there were significant deviations of experimental performance from theoretical performance. The experimental characteristic velocity was greater than the theoretical values while the experimental specific impulse was significantly lower. Before data could be reported in final form, several factors effecting the deviations of the experimental engine performance from the theoretically computed values had to be explored and evaluated. The deviations investigated were:

1) calibration of the thrust measuring load cell
2) thrust losses due to static and dynamic effects of the propellants passing through the manifold
3) thrust losses due to a nozzle expansion section discontinuity
4) variation of C* due to throat erosion

1. To accurately calibrate the thrust stand, two identical hydraulic actuators were installed symmetrically behind the load cell. By pressurizing the actuators simultaneously, an evenly distributed simulated thrust could be applied to the test stand and load cell. Any portion of the load which

was absorbed by the stand and not measured by the load cell could therefore be evaluated. The load cell was tested from 4000 lbs tension to 7000 lbs compression and an error of approximately 6.8% was found in the previous technique of load cell calibration (see Fig. 1).

The previous technique applied a load through a lever arm and resulted in some hysteresis. The tabulated recalibration is given below.

Actuator Load Applied (lbs)	Load Cell Output (m.v.)	Previous Loader Force (lbs)	Previous Load Cell Output (m.v)	Corrected Loader Force (lb)
0	0			
1984.3	1113	2535	1525	2686.3
3968.5	2263	7336.	4382	7718.9
5957.8	3365	7336	4383	7720.6
7937	4508	2535	1543	2718
3968.5	2264			
0	0			
- 322.7	- 179			
- 806.6	- 443			
-1613.5	- 895			
-3227.0	-1840			
-6454	-3670			
0	0			

2. To evaluate the bourbon effects or stiffening of the system due to high (4000 psi) pressure and the effects of momentum change as the propellants passed through the manifold system prior to injection, a theoretical model of the system was first analyzed. This analysis showed that the dynamic effects were one order of magnitude smaller than the static pressure effects.

By calibrating the load cell, with and without the manifold lines pressurized, the static pressure effects were shown to be less than .1%. The static pressure and dynamic flow losses were therefore neglected. Subsequent analysis of the start cycle of the experimental firings during which time oxidizer only was flowing (oxidizer lead) reconfirmed that the static and dynamic effects could be neglected.

3. A nozzle discontinuity was discovered to result from a miss matching of nozzle expansion sections. The flow at the discontinuity was supersonic and separation and shock losses were suspected. The losses due to a Prandtl Meyer expansion and separation were evaluated to be approximately 3.4 and 3.57% respectively. The analysis assumed the flow expanded to a vacuum at the discontinuity, that a local shock formed at the flow turning point downstream of the discontinuity thus triggering flow separation, and that the separated flow did not re-attach within the remaining portion of the nozzle. These assumptions are being further analyzed both here and at NASA Lewis Research Laboratories to determine the validity of a thrust correction for the separation effect.

4. Further investigation into the deviation of experimental C* from theoretical C* indicated the desirability of examining the variation of throat area with time. The analysis which evolved determined the experimental variation in "effective" throat area as a function of time during the steady state portion of the experimental firings. And then fitted this variation to intersect the "actual" post fire throat area at shut down. "Actual" is used to denote the measurable area of the nozzle throat and "effective denotes the throat area experienced by the flow. The differ-

ence between actual and effective areas can result from the flow of ablated chamber material which reduces the flow area, and the thermal and compressive properties of the ablative nozzle which tend to increase the flow area. During steady state it is expected that the deviation between effective and actual area should stabilize, in which case fitting the area variation to the post-fire condition results in the determination of actual area variation rather than the area experienced (effective area) by the flow of combustion gases (Fig. 5).

To determine the "effective" area, Dr. Priem has suggested that experimental runs be made with both copper and ablative nozzles at lower pressures of 1000 psi, 2000 psi, and 3000 psi in an attempt to reduce the throat area uncertainty caused by the ablative nozzle. The isp and C* efficiencies will then be plotted versus chamber pressure to correlate and extrapolate the relation to a chamber pressure of 4000 psi. This technique will enable the calculation of the performance of a rocket engine at 4000 psi without the effects of the ablative material used to line the chamber.

The procedure presently used to calculate the "actual" throat area is as follows:

1) Assume steady state combustion results in an experimental C* which does not vary appreciably from a mean value. This was found true for the theoretical C*. For this case (Fig. 5)

1) $C_1^* = g \dfrac{P_{c_1} A_1}{\dot{w}_1}$

2) $C_2^* = g \dfrac{P_{c_2} A_2}{\dot{w}_1}$

where P_c = chamber pressure
A = throat area
$\dot{w}$ = propellant flow rate

and thus (see Fig. 3)

3) $\dfrac{A_1}{A_2} = \dfrac{C^*_1}{C^*_2} \dfrac{\dot{w}_1}{\dot{w}_2} \dfrac{P_{c_2}}{P_{c_1}} \approx \dfrac{\dot{w}_1}{\dot{w}_2} \dfrac{P_{c_2}}{P_{c_1}}$

thus the ablation rate "K" is given by

4) $K = \dfrac{dA}{dt} = \dfrac{A_2 - A_1}{t_2 - t_1} = \dfrac{A_2}{t_2 - t_1} \left[1 - \dfrac{A_1}{A_2} \right] = \dfrac{A_2}{t_2 - t_1} \left[1 - \dfrac{\dot{w}_1}{\dot{w}_2} \dfrac{P_{c_2}}{P_{c_1}} \right]$

if one lets t_2 be t_f (shut down)

5) $K = \dfrac{A_F}{t_2 - t_1} \left[1 - \dfrac{\dot{w}_1}{\dot{w}_2} \dfrac{P_{c_2}}{P_{c_1}} \right]$

If one further assumes that the shut down is abrupt (Fig. 4) then A_f is equal to the postfire area. Thus all the terms on the right side of equation 5 are known data and therefore K is determined.

The actual nozzle throat area becomes

6) $A(t) = A_{t_{\text{shut down}}} - k[t_{\text{shut down}} - t]$

Because C* and Isp calculations are not valid for the transient period of start up, the area variation is only used for steady state calculation where the linear variation is defined.

In summary, several avenues of analysis are being investigated so that the performance data recorded during the first 24 experimental firings will accurately reflect the performance of a rocket engine operated at 4000 psi with the injector configurations and characteristic lengths employed. To do this, the thrust stand was calibrated to eliminate experimental errors caused by the thrust which was not totally sensed by the load cell, dynamic and static forces applied through the manifold lines were determined to be negligible, thrust losses due to a discontinuity in the expansion portion of the nozzle have been estimated, and the throat area variation with time will be determined. In addition experimental firings with the copper nozzle will establish the effects of ablation which are not readily calculated such as the compressive, thermal and mass addition effects.

B. Task 2. Heat Transfer Investigation

The calorimeter technique proposed by R. L. Schacht, R. J. Quentmeyer and W. L. Jones has been chosen as the primary method to be employed in measuring heat transfer rates in the experimental rocket engine. Theoretical calculations predict that calorimeters would not withstand the nozzle throat heat flux if the engine were operated above 3000 psi chamber pressure with a contraction ratio of 5.5. Therefore experimental engine firings will be made at 1000, 2000, and 3000 psi using the calorimeter and the copper nozzle to determine the heat flux at the throat and at several positions along the

wall, and then firings will be repeated at 1000, 2000, 3000, and 4000 psi using ablative nozzles. Two correlations will be made.

The first correlation will be between the chamber and nozzle heat flux for varying chamber pressure. By extrapolating the first correlation to 4000 psi where the chamber heat flux is still measurable, the nozzle throat heat flux will be determined (see Fig. 7).

The second correlation will be between nozzle ablation and nozzle heat flux (Fig. 8) for varying chamber pressure. By correlating nozzle ablation and heat transfer rates at lower pressures and extrapolating the results to higher pressures at which nozzle ablation tests can still be conducted; it will be possible to approximate the actual rate of heat transfer at 4000 psi chamber pressure (see Fig. 8). A preliminary investigation suggested that the throat area variations determined for performance calculations will be applicable to heat transfer investigation. The throat area variation is directly related to ablation rate, i.e.

$$K = f_1 \frac{dm}{dt}$$

The ablation rate is directly related to the concentration gradient across the boundary layer (Fig. 9), i.e.

$$\frac{dm}{dt} = f_2 [\Delta c]$$

and the concentration gradient is related to the heat input, i.e.

$$\Delta c = f_3 (\dot{Q})$$

thus

$$\dot{Q} = f_3^{-1}\left[f_2^{-1}\left[f_1^{-1}(K)\right]\right] = f_4(K)$$

Ablation rates are therefore being recorded as pertinent data. Fur use in calculating nozzle heat flux as well as to report the performance of the ablative nozzles and chamber liners used on this program.

C. Task 3. Combustion Stability Investigation

The objective of this investigation is to pulse the experimental rocket engine (Fig. 10) and determine the stability bounds at 4000 psi chamber pressure. Three pulsed firings will be made for each of three mixture ratios (O/F = 1.7, 2.0, 2.3), two injector configurations (large and small droplet size), and two chamber L* (50 and 100). Thirty six firings are anticipated as necessary to accomplish the task.

For reporting purposes the combustion stability investigation will be divided into three phases of development:

1) Pulse gun design modification for high pressure application.
2) Pulse gun sequence triggering system
3) Pressure sensing instrumentation

1) The first phase may be divided into several stages of pulse gun modification to withstand high chamber pressure, each aimed at improving the safety, durability or reliability of a system during a pulsed experimental firing.

a. To eliminate the possibility of a burn-out of the engine in the event the pulse gun was extruded, it was decided to tatally enclose the

pulse gun in a stainless steel capped cylinder (Figs. 12 and 13). The height of the cylinder is low enough such that the pulse gun could not fully extrude and is high enough to provide room for an electrical connection. An insulated terminal passing through the cylinder wall provides the 2000 volt lead required for detonation, and the entire engine forms the ground terminal.

b. To prevent combustion gases from entering the retaining cylinder, the cylinder is pressurized with nitrogen (Fig. 13) to a pressure greater than the combustion pressure. Thus no escape of combustion gases is possible.

c. To avoid fracturing the ablative liner of the engine (Fig. 13), a stainless steel shieth was fabricated to surround the pulse gun forming a wall between the ablative liner and the explosive charge.

d. Upon pressurization of the retaining cavity is was found that the electrical terminal passing through the pulse gun to the detonator could leak and slowly extrude the explosive wafers. To prevent this leak a cap was fabricated to enclose the pulse gun terminal (Fig. 14). However, shorting in the cap and recurrent leaking was sometimes observed. To eliminate these problems the cap was removed and a small passage was drilled into the pulse gun and steel shieth allowing leaking nitrogen to escape before extruding the explosive charge.

e. To retard the rate at whichheat was conveyed from the combustion gases to the explosive charge, zinc chromate paste was employed to fill the one inch gap between the teflon cap containing the explosive charge and the combustion chamber. This, did not sufficiently reduce the heat transfer, however. A frangible ablative plug was therefore placed within the zinc

chromate as a final wall between the combustion gases and the explosive charge (Fig. 14).

f. Because an escape path was not readily formed for leaking nitrogen, a steel pin was inserted through the shieth to hold the ablative plug in place, and epoxy cement sealed the pin and plug. Sealing the pluse gun in this manner forced leaking gases to take the alternate route up through the steel shieth and down into the chamber.

g. Finally, to eliminate the possibility of the combustion gases burning through the pin and allowing the ablative plug to be dislodged permitting extrusion, the pin was recessed 3/4 inch from the chamber inner wall.

2) To initiate the detonation of the pulse gun the following circuitry was employed:

a) The engine sequencing circuit (see Fig. 15) controls the timing of the propellant value actuations and hence the run duration. Upon opening the fuel valve the fuel valve position switch is closed providing a 28 volt source for a transistor triggered timer.

b) The resistances and capacitors of the timer may be adjusted to provide the necessary delay between when the engine starts up and when steady state combustion is achieved (Fig. 16).

c) When the timer times out, a relay closes and a 2000 voltage supply discharges into the detonator causing detonation of the explosive wafers. Each step in the sequence is monitored by recording the voltage drop across a resistor in the appropriate circuit (see Fig. 16) and recorded for run analysis.

d) During the first five experimental firings it was found that the delay timer (Fig. 15) was not timing out and therefore the pulse gun was not firing. This problem was eliminated when it was discovered that the timer's power source was taken through the valve micro-switch which broke contact due to the engine vibration. To solve this problem the micro-switch power was used to energize a relay across which a capacitor was placed. The relay in turn closed the circuit for the delay timer.

3) The pressure sensing instrumentation is vital to the determination of stability criterion. A photocon transducer was chosen for the purpose of sensing the steep pressure rise associated with the shock formed upon detonation of the pulse gun. The photocon transducer response was specified as linear from 2 cps to 16,000 cps. As a result of the high response to low frequencies, the slow variation in photocon capacitance due to heat transfer caused a substantial drift in the photocon transducer output. This drift was countered by changing a circuit capacitor, thus limiting the low frequency response to 50 cps.

The first successful pulsing of the engine resulted in a 428 psi pressure transient. The transient did not include a sharp pressure rise such as a shock wave would produce. This has raised a question about the sensitivity of the photocon transducer and the design of the pulse gun. A significant mass has been added to the pulse gun to prevent heat transfer and extrusion of the explosive charge by leakage of the nitrogen pressurized cylinder (Fig. 13). Whether or not this mass prevents shock formation will be determined by the next report.

III. PLAN FOR FUTURE RESEARCH

1) To account for the effects of ablation on the performance of the engine, an attempt will be made to isolate those factors introduced by ablation. This will be carried out as stated previously by fabricating a copper nozzle and comparing the performances at 1000, 2000, and 3000 psi of a non-ablating and an ablative nozzle. The deviation in performance will be ascribed to the effects of ablation and the resulting correction factor will be plotted as a function of chamber pressure and extrapolated to 4000 psi. This final correction will then be applied to the data from the initial 24 runs.

2) To determine the suitability of the present pulse gun and photocon transducer, the engine will be pulsed with both a photocon and a kistler transducer. If no pulse is recorded by either the pulse gun will be re-modified. If the kistler registers the shock but the photocon transducer does not, the photocon circuit will be re-examined. If both the photocon transducer and pulse gun perform well, the engine will be pressurized similar to engine start up and the engine will once again be pulsed. When all components have been tested, live pulsed firings will commence again.

3) A single quadlet element injector will be fabricated with the option of having an uncooled face plate or a transpiration cooled face plate. This injector will be used to obtain additional performance and stability data and in conjunction with a study of the temperature profiles of the injected propellants as the combustion proceeds within the chamber.

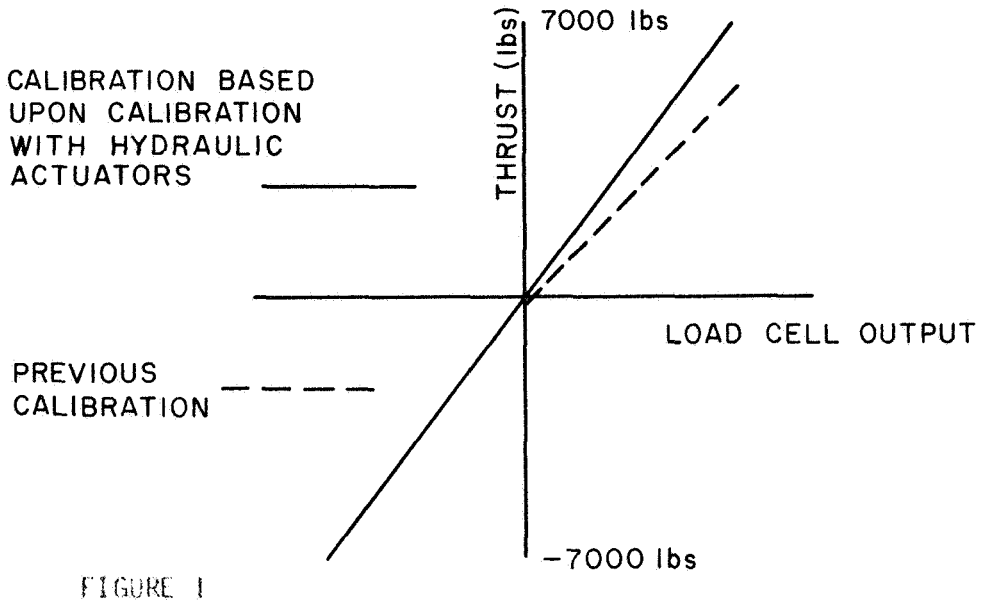

FIGURE 1
Calibration Correction

The load cell was recalibrated with hydraulic actuators to simulate the actual thrust loading of the test stand.

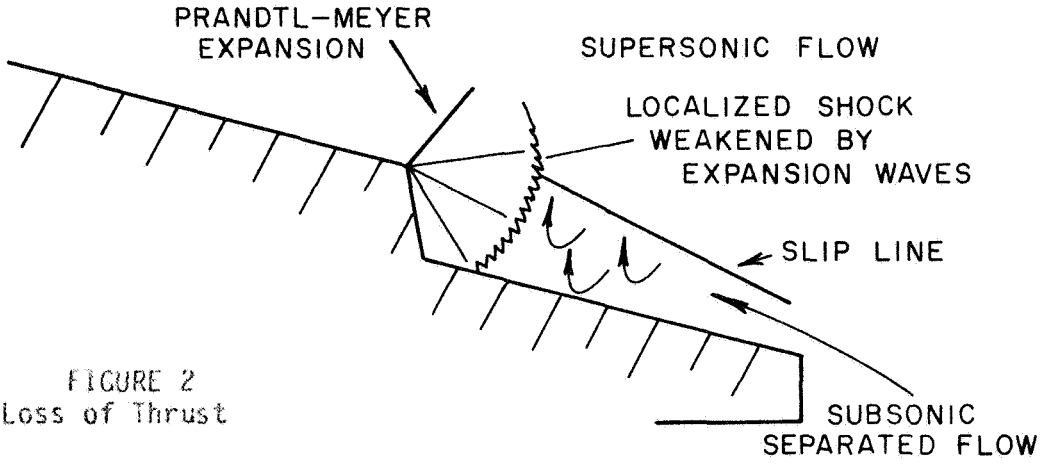

FIGURE 2
Loss of Thrust

The nozzle discontinuity causes a loss of pressure acting on the area of the discontinuity as well as a shock which initiates flow separation.

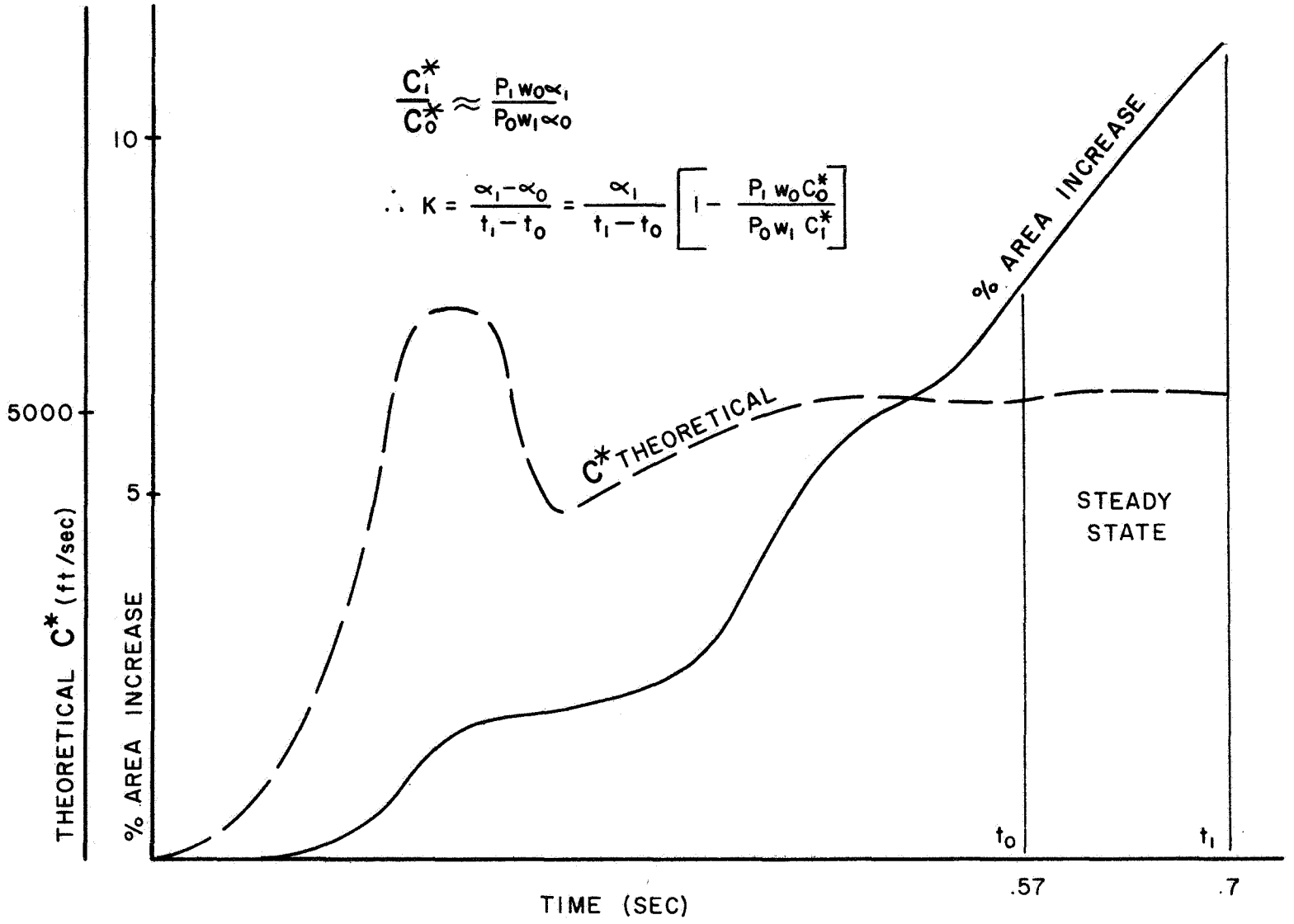
$\frac{C_1^*}{C_0^*} \approx \frac{P_1 w_0 \alpha_1}{P_0 w_1 \alpha_0}$
$\therefore K = \frac{\alpha_1 - \alpha_0}{t_1 - t_0} = \frac{\alpha_1}{t_1 - t_0}\left[1 - \frac{P_1 w_0 C_0^*}{P_0 w_1 C_1^*}\right]$
10
5000
5
THEORETICAL C* (ft/sec)
% AREA INCREASE
C* THEORETICAL
% AREA INCREASE
STEADY STATE
t_0
t_1
.57
.7
TIME (SEC)

FIG. 3

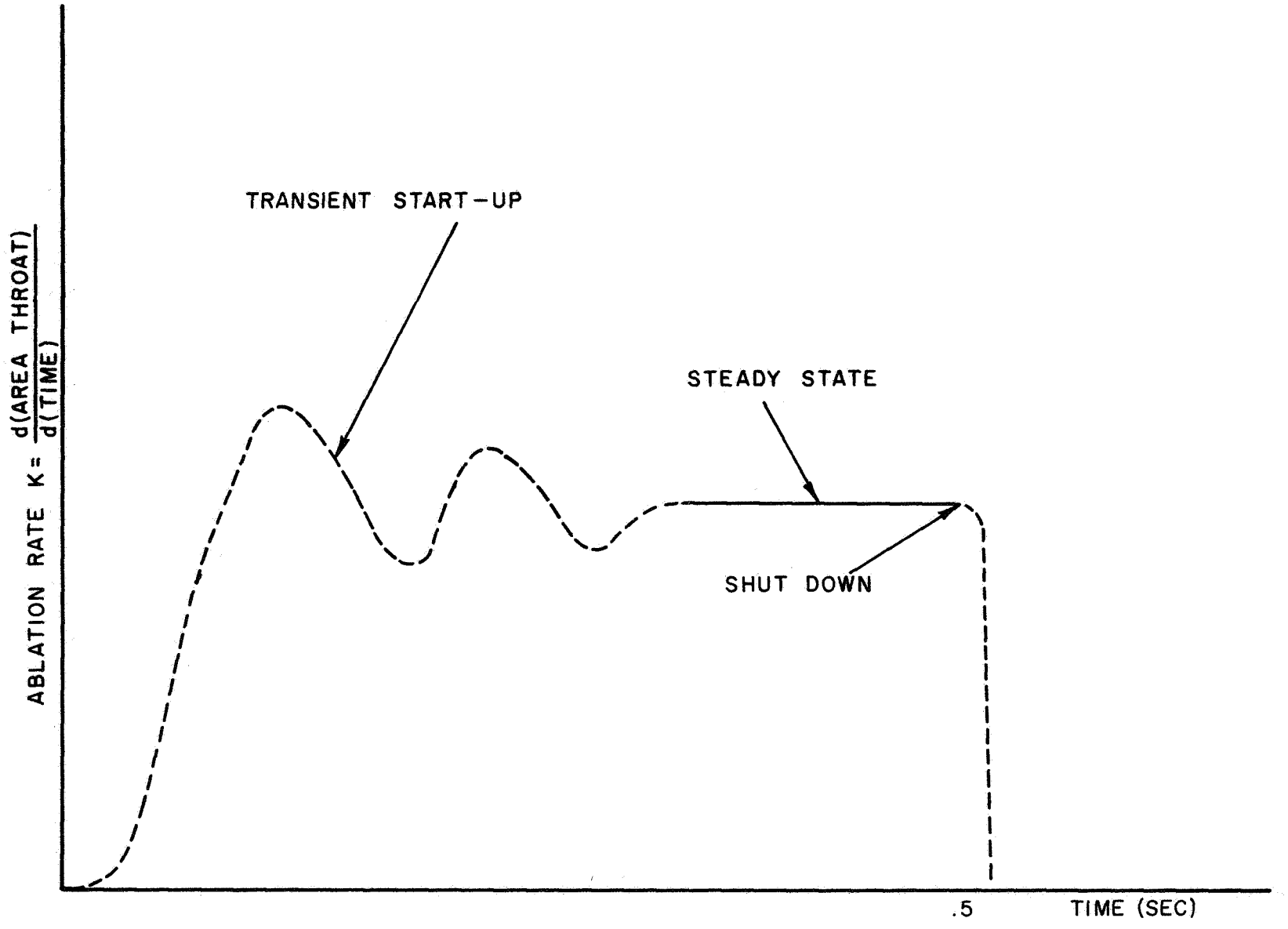
ABLATION RATE K= d(AREA THROAT) / d(TIME)
TRANSIENT START-UP
STEADY STATE
SHUT DOWN
.5
TIME (SEC)

FIG. 4

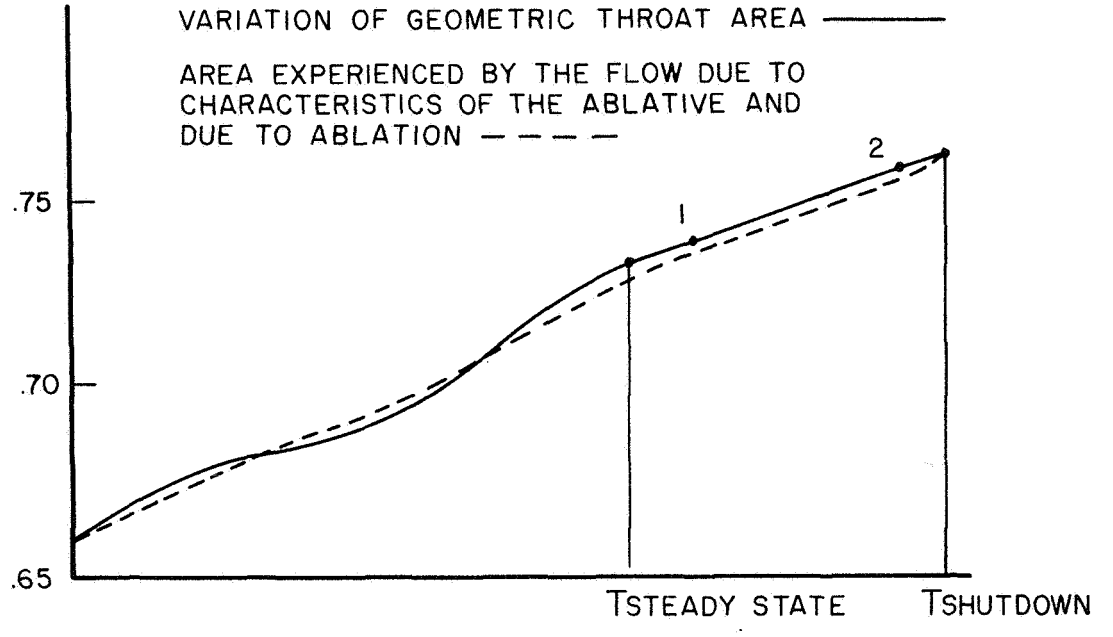
VARIATION OF GEOMETRIC THROAT AREA
AREA EXPERIENCED BY THE FLOW DUE TO CHARACTERISTICS OF THE ABLATIVE AND DUE TO ABLATION
.75
.70
.65
1
2
TSTEADY STATE
TSHUTDOWN

FIGURE 5

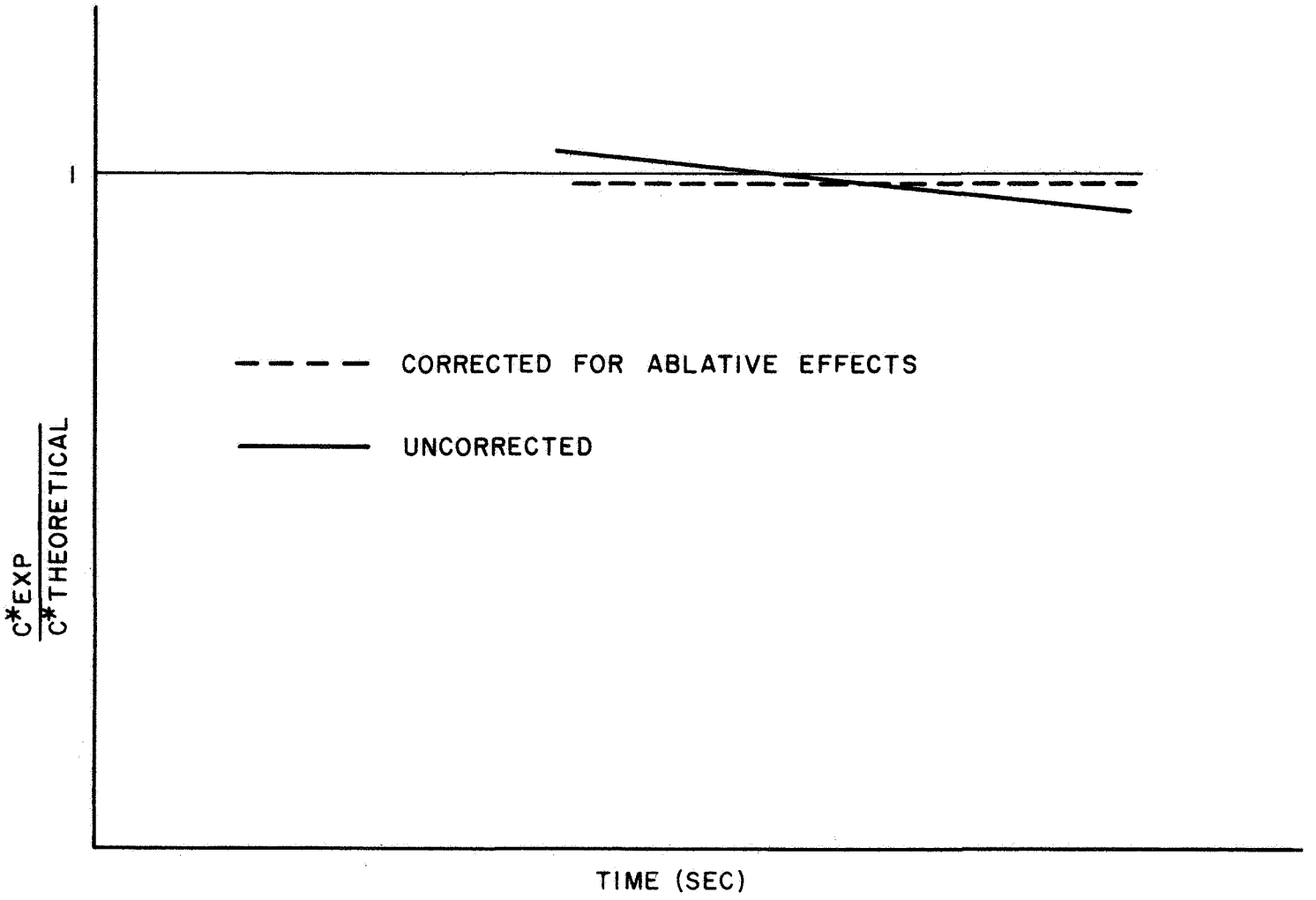
1
CORRECTED FOR ABLATIVE EFFECTS
UNCORRECTED
C*EXP / C*THEORETICAL
TIME (SEC)

FIG. 6

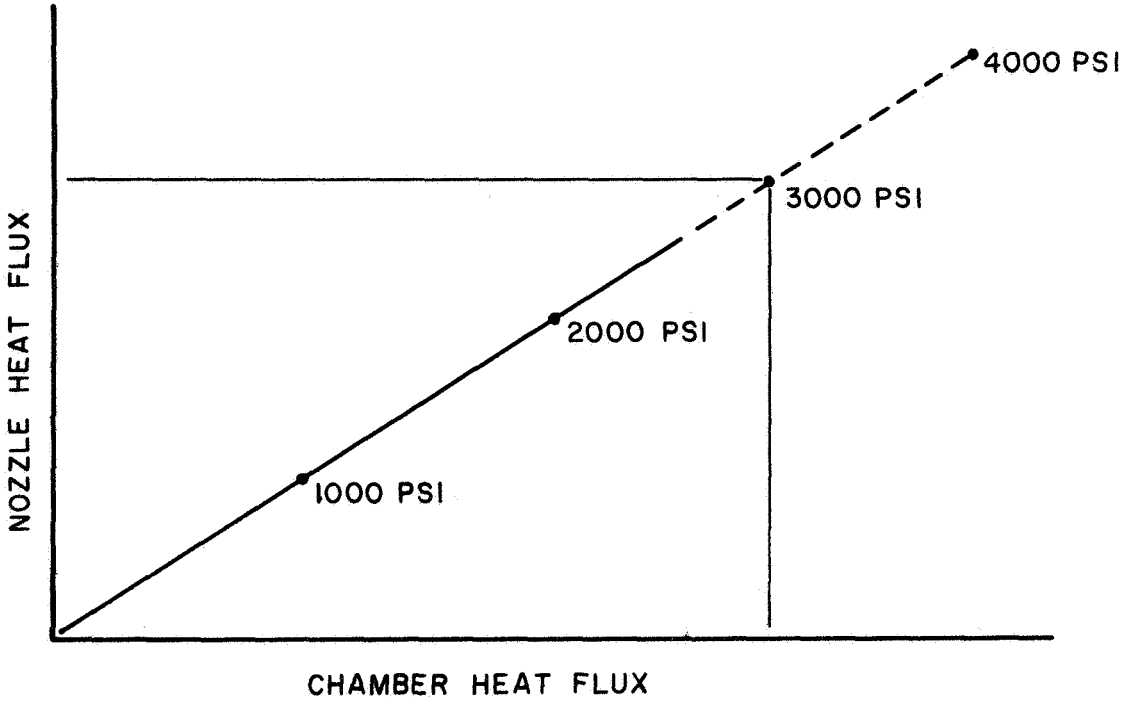

FIG. 7

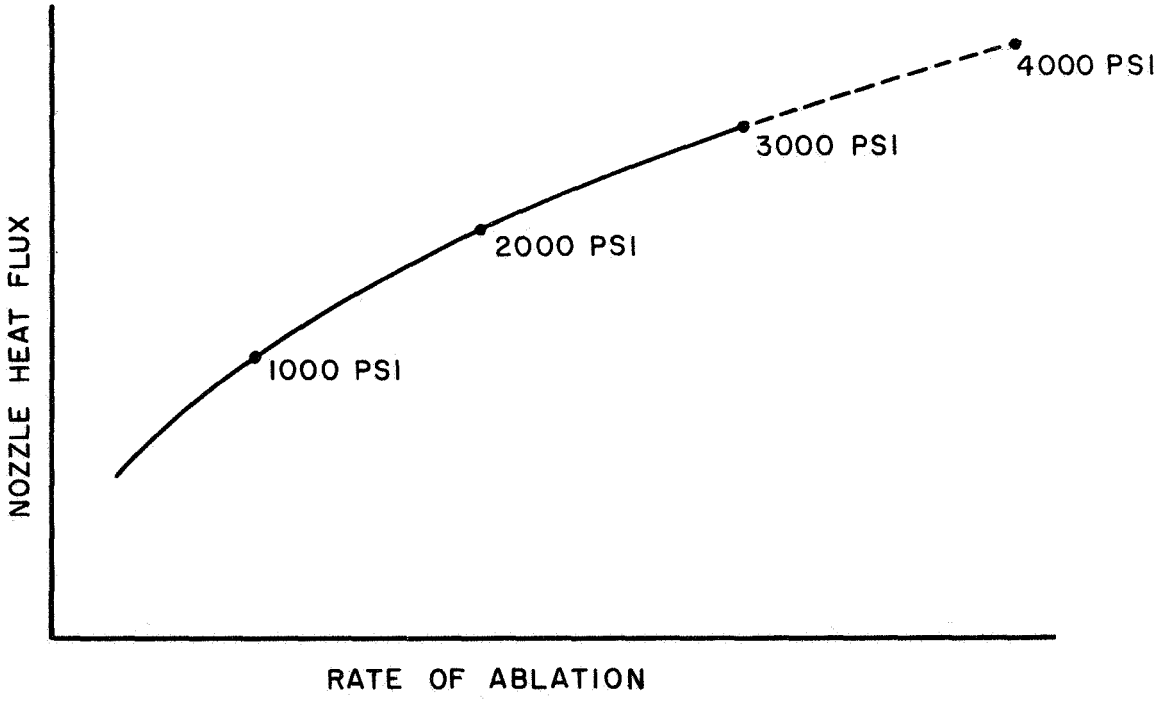

FIG. 8

TWO METHODS FOR DETERMINING HEAT FLUX AT 4000 PSI

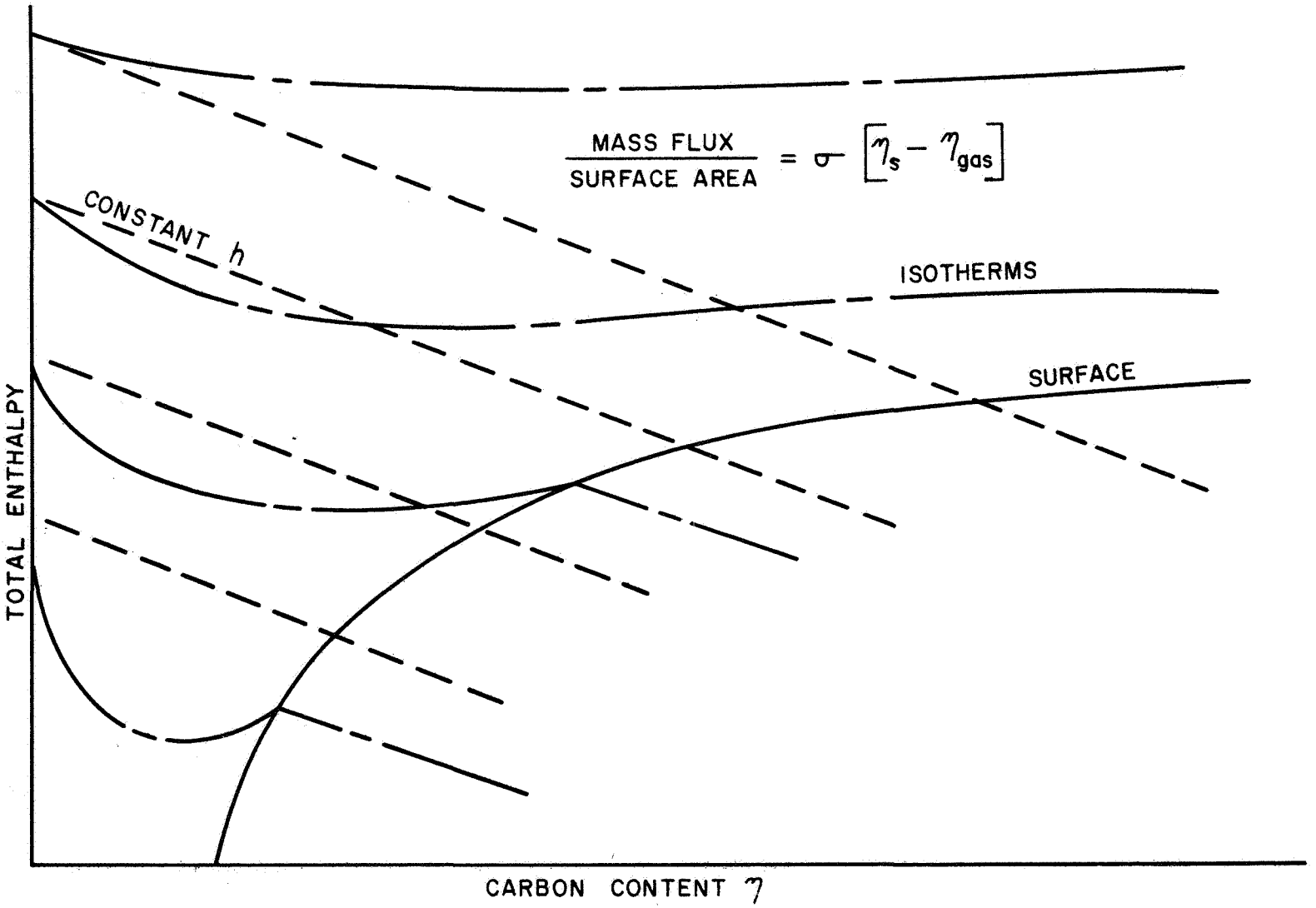
MASS FLUX / SURFACE AREA = σ [η_s − η_gas]
CONSTANT h
ISOTHERMS
SURFACE
TOTAL ENTHALPY
CARBON CONTENT η

FIG. 9

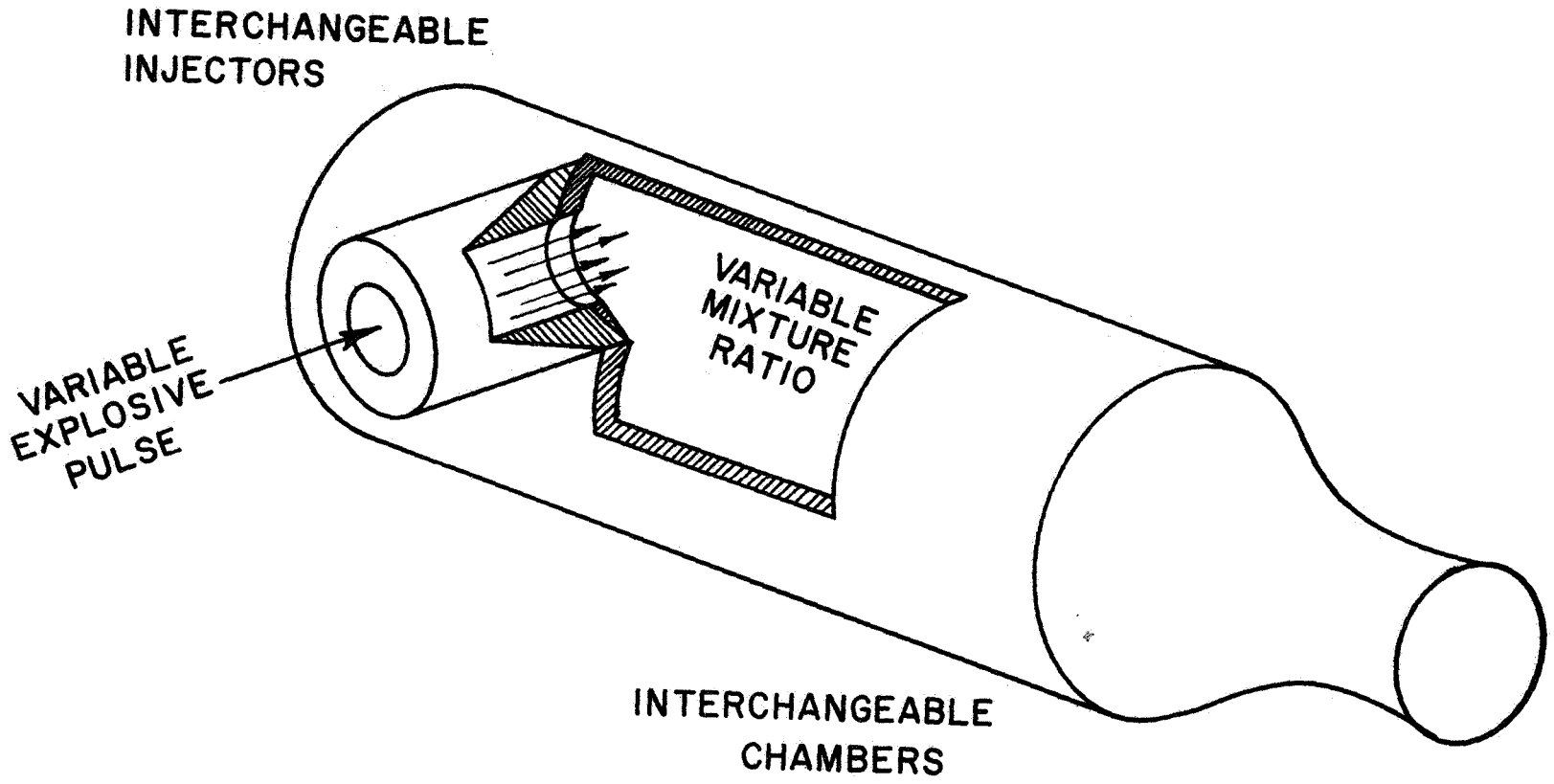
INTERCHANGEABLE
INJECTORS
VARIABLE
EXPLOSIVE
PULSE
VARIABLE
MIXTURE
RATIO
INTERCHANGEABLE
CHAMBERS

FIG. 10

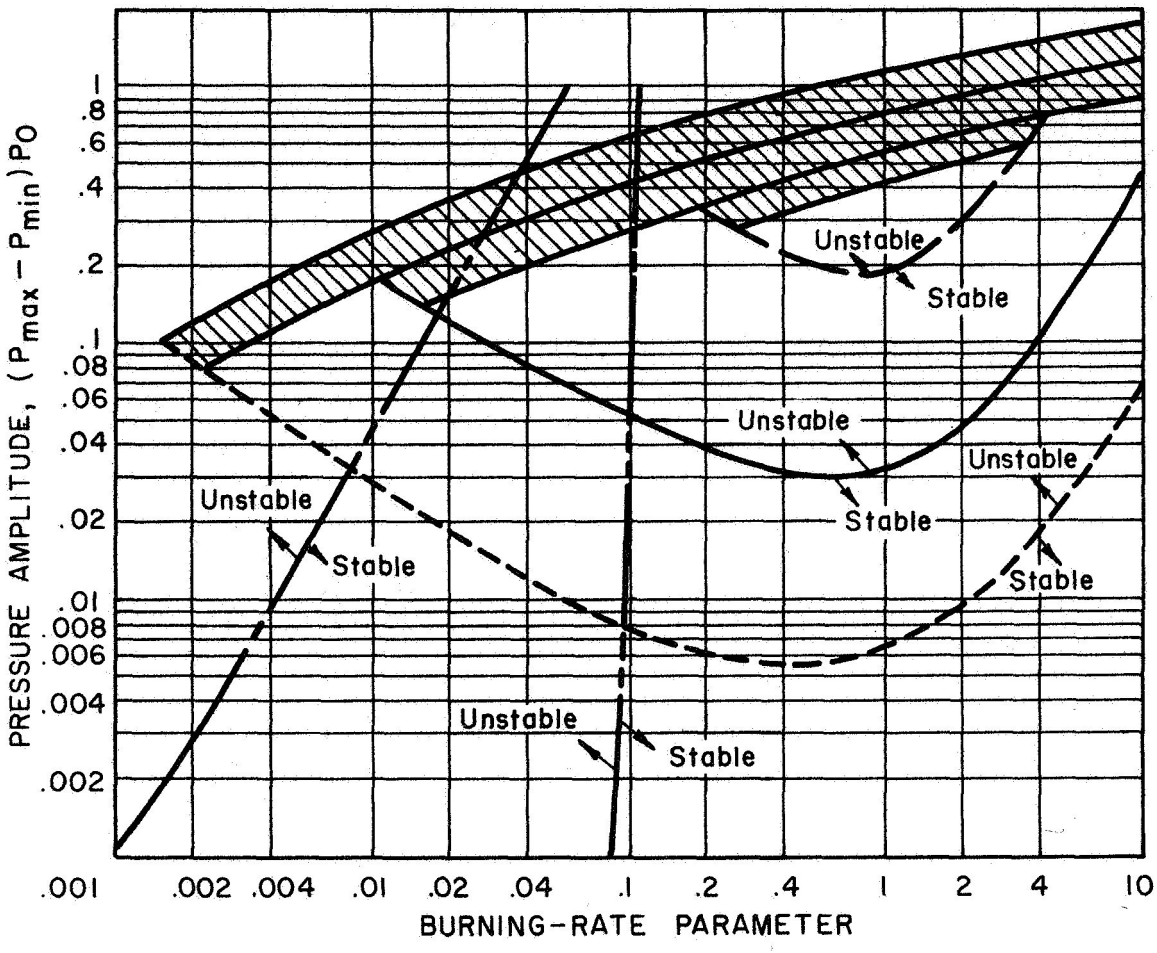

REDUCED VELOCITY DIFFERENCE BETWEEN GASES AND DROPS IN AXIAL DIRECTION, ΔV

— — .04
——— .02
- - - - - .01

VAPORIZATION RATE MODEL

AVERAGE MOLE FRACTION CONCENTRATION OF UNBURNED GASES, C_O

— - — .01
— - - — .1

CHEMICAL-REACTION RATE MODEL

▨ FINAL AMPLITUDE OF THE INSTABILITY

FIG. 11

COMPARISON OF STABILITY LIMITS FOR VAPORIZATION-RATE AND CHEMICAL-REACTION-RATE MODELS.

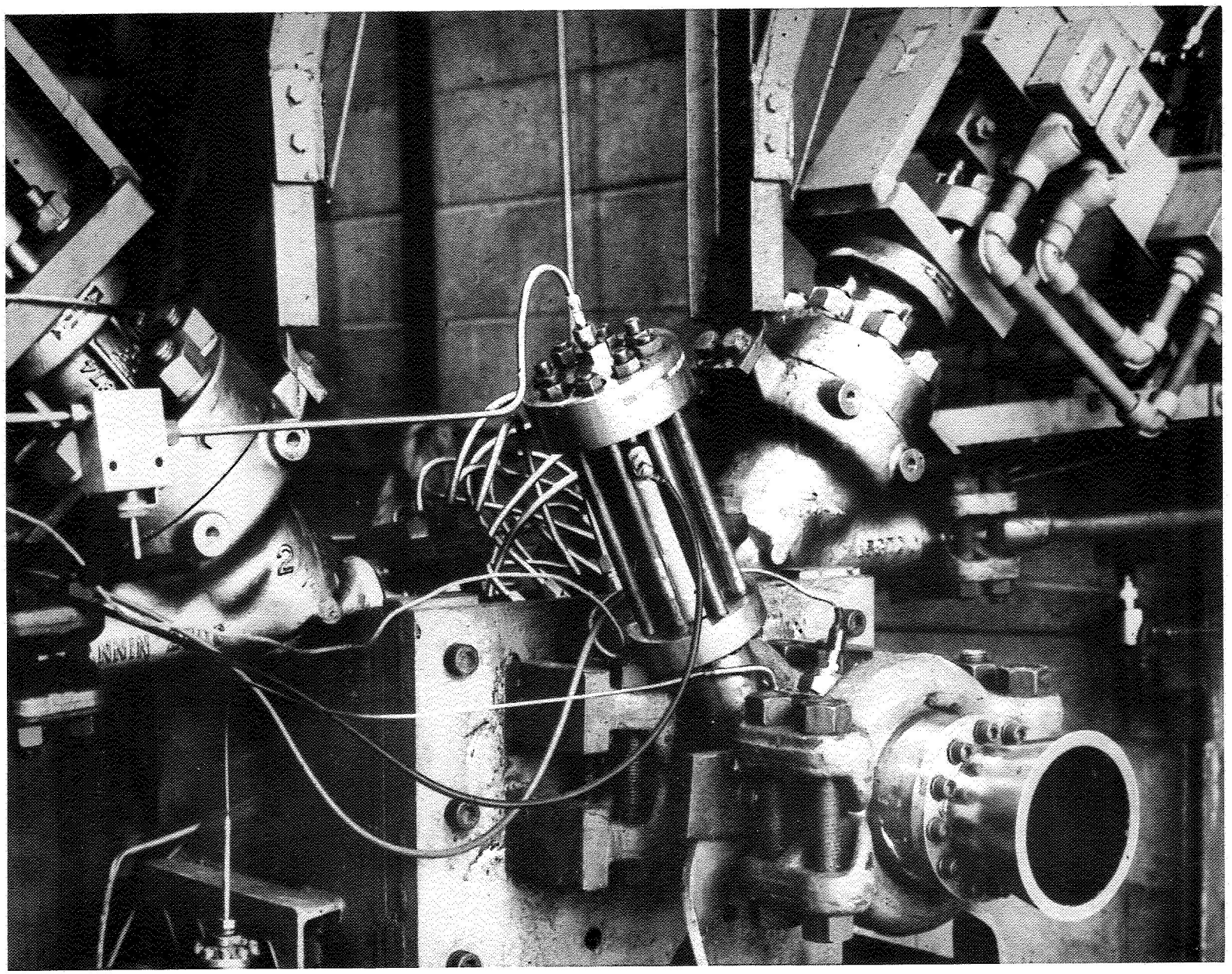

FIGURE 12
EXPERIMENTAL ROCKET MOTOR

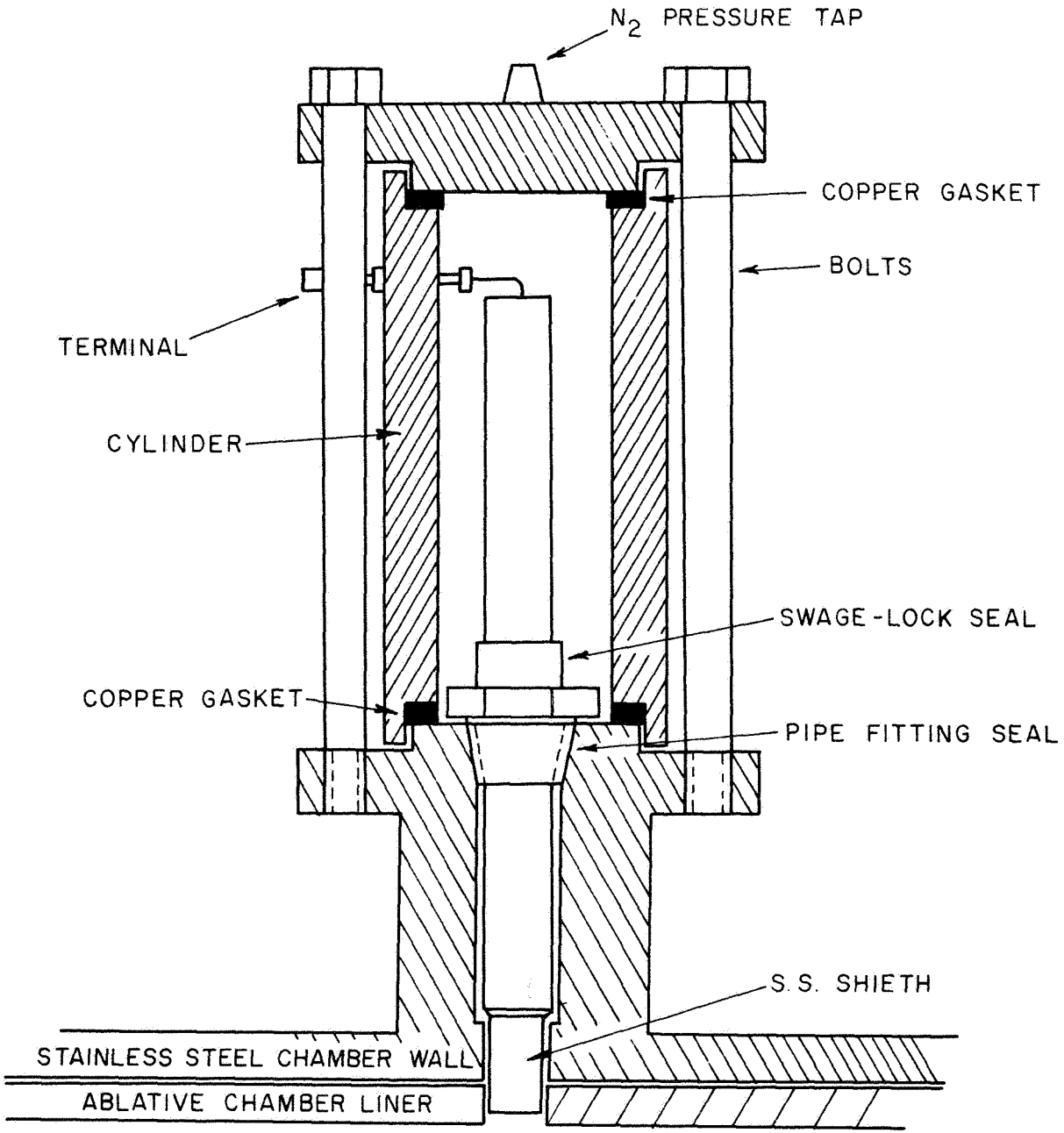
N_2 PRESSURE TAP
COPPER GASKET
BOLTS
TERMINAL
CYLINDER
SWAGE-LOCK SEAL
COPPER GASKET
PIPE FITTING SEAL
S.S. SHIETH
STAINLESS STEEL CHAMBER WALL
ABLATIVE CHAMBER LINER
COMBUSTION CHAMBER

FIGURE 13

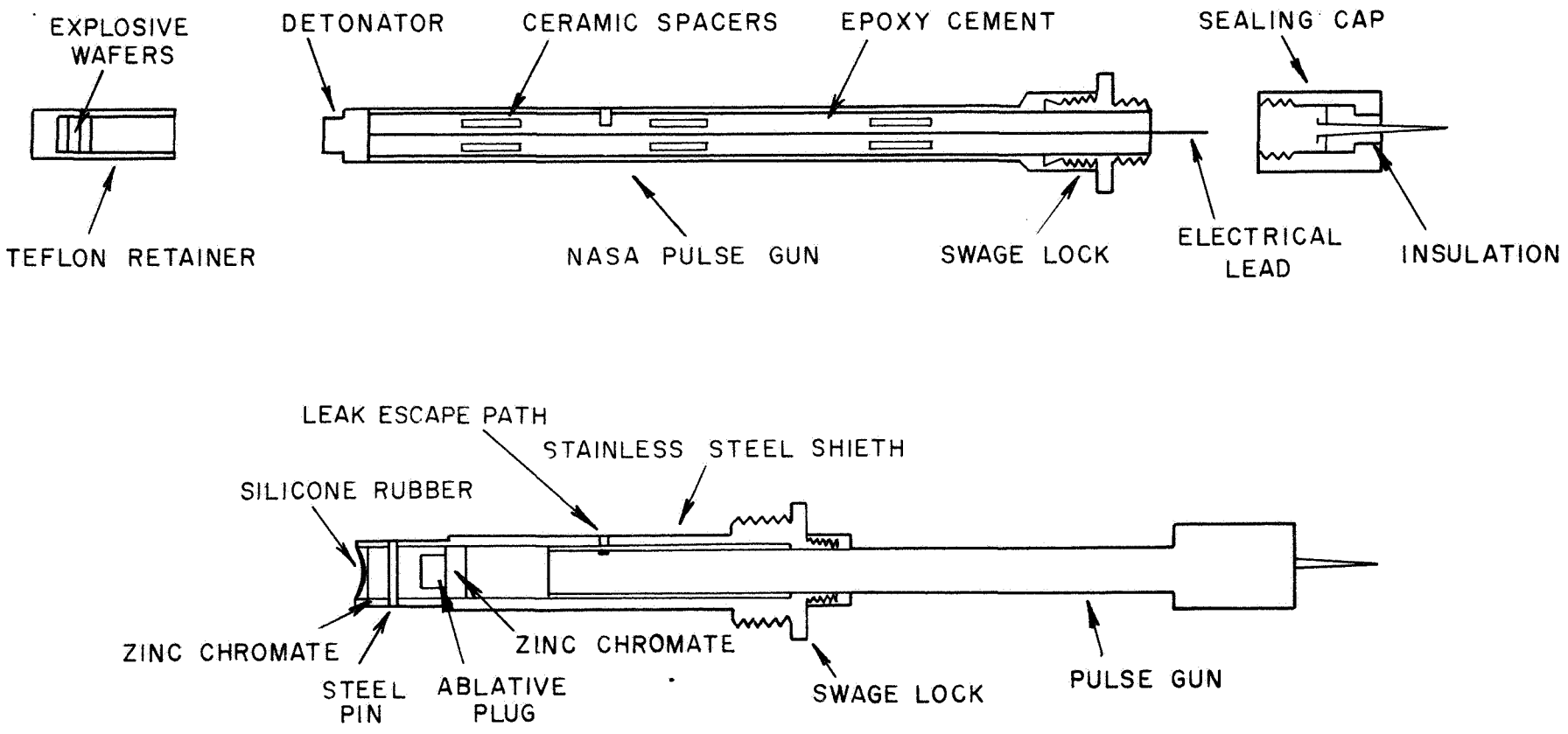
EXPLOSIVE WAFERS
DETONATOR
CERAMIC SPACERS
EPOXY CEMENT
SEALING CAP
TEFLON RETAINER
NASA PULSE GUN
SWAGE LOCK
ELECTRICAL LEAD
INSULATION
LEAK ESCAPE PATH
STAINLESS STEEL SHIETH
SILICONE RUBBER
ZINC CHROMATE
ZINC CHROMATE
STEEL PIN
ABLATIVE PLUG
SWAGE LOCK
PULSE GUN

FIG. 14

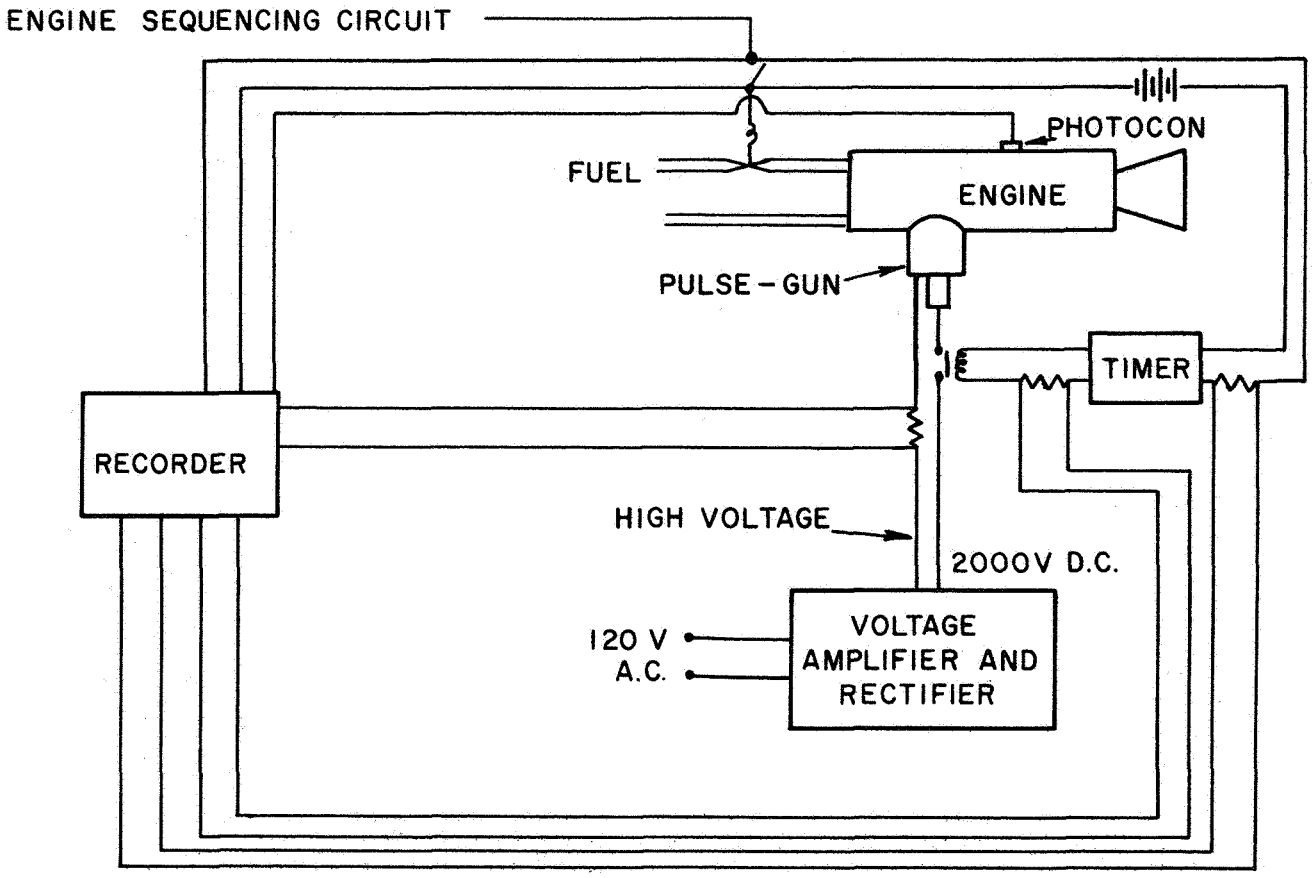

PULSE-GUN SEQUENCING AND
DETONATION CIRCUITS

FIG. 15

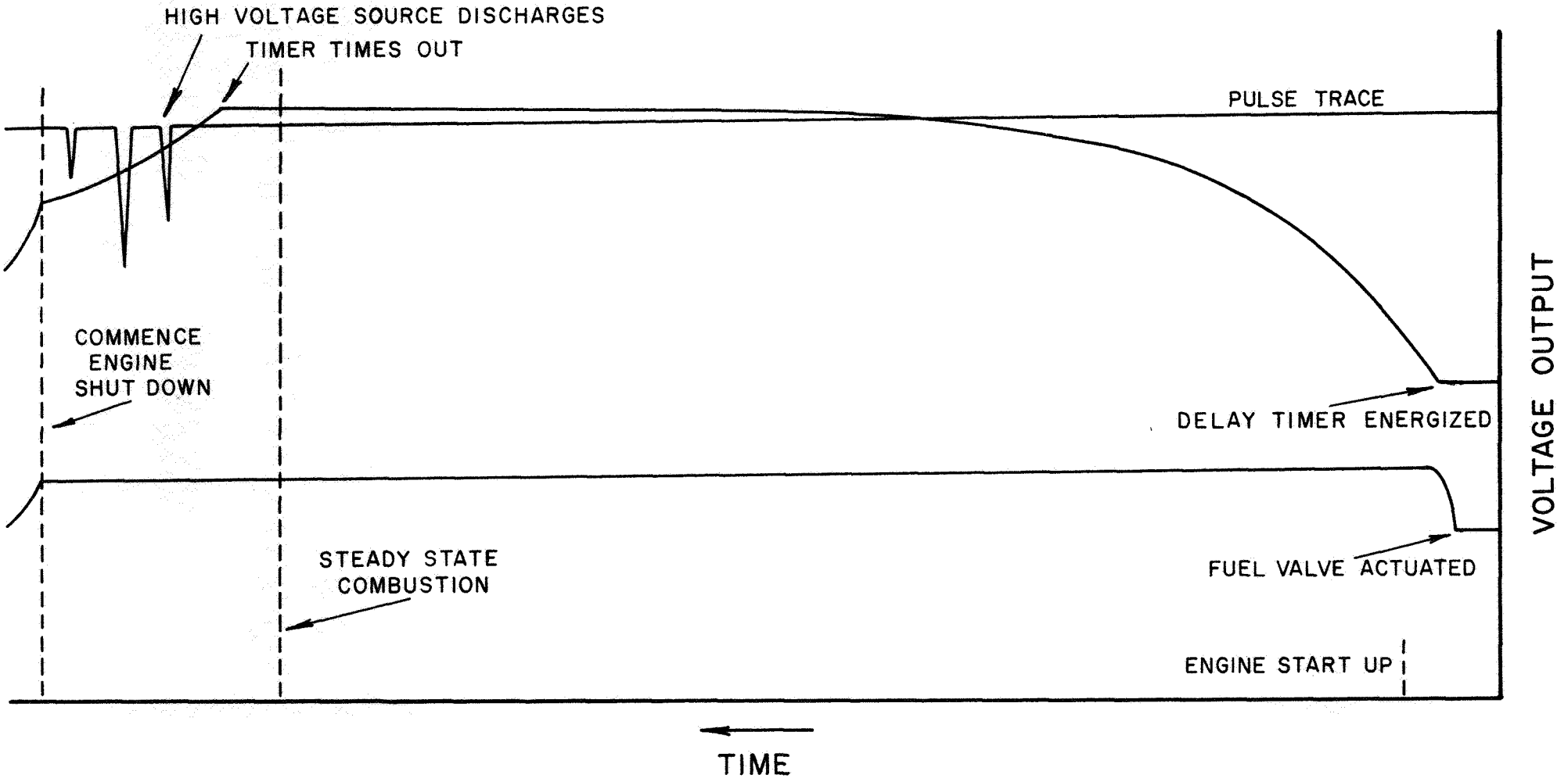
HIGH VOLTAGE SOURCE DISCHARGES
TIMER TIMES OUT
PULSE TRACE
COMMENCE ENGINE SHUT DOWN
DELAY TIMER ENERGIZED
STEADY STATE COMBUSTION
FUEL VALVE ACTUATED
ENGINE START UP
VOLTAGE OUTPUT
TIME

FIGURE 16